Multi-objective inversion of surface waves and receiver functions by competent genetic algorithm applied to the crustal structure of the Paraná Basin, SE Brazil

Meijian An and Marcelo S. Assumpção

Department of Geophysics, IAG, University of São Paulo, São Paulo, SP, Brazil

Received 27 November 2003; revised 16 January 2004; accepted 22 January 2004; published 13 March 2004.

[1] Surface wave dispersion and receiver functions are sensitive to different, but dependent, seismic properties. Their joint inversion is multi-objective and can provide tight constraints on layer-interfaces and S-velocities. We used one of the competent genetic algorithms, Bayesian optimization algorithm, as the multi-objective inversion technique. Multi-objective criterion of receiver functions and surface wave dispersion can better constrain solutions than each separate objective. We applied this new method to data from three stations in the Paraná Basin, Brazil, and found S-velocity structure well-constrained down to 150 km depth. The inverted S-velocities in the lower crust are less than 3.8 km/s and are lower than in the surrounding foldbelts. Some indication of high velocities (Vs > 4 km/s) in the 5–7 km lowermost crust is given by a Moho transition zone. This may suggest that possible underplating was not widespread in the Paraná basin. *INDEX TERMS:* 3260 Mathematical Geophysics: Inverse theory; 7218 Seismology: Lithosphere and upper mantle; 7255 Seismology: Surface waves and free oscillations; *KEYWORDS:* multi-objective optimization, surface wave, receiver function, crustal structure, Brazil. **Citation:** An, M., and M. S. Assumpção (2004), Multi-objective inversion of surface waves and receiver functions by competent genetic algorithm applied to the crustal structure of the Paraná Basin, SE Brazil, *Geophys. Res. Lett.*, *31*, L05615, doi:10.1029/2003GL019179.

1. Introduction

[2] Surface wave dispersion (SWD) is sensitive to depth-average S-velocity. Receiver function (RF) is primarily sensitive to body wave velocity contrasts and vertical travel times. So, SWD and RF constrain different, but dependent, seismic properties of the crustal structure and their joint inversion can provide tight constraints on both discontinuities and S-velocities. Joint inversions have previously been done by linearized method [e.g., *Özalaybey et al.*, 1997; *Julià et al.*, 2000]. The joint inversion, in fact, is a multi-objective problem with more complex nonlinearity than the single-objective problem of SWD or RF. The main challenges in a nonlinear inversion are to find the best solutions as well as good solutions extending over the acceptable model-space and objective-space. These challenges require both a competent inversion technique and an appraisement among all acceptable models but not only among several best models. Being a local algorithm, the traditional linearized method can not easily satisfy these requirements.

0094-8276/04/2003GL019179$05.00

[3] Genetic algorithm (GA) operates on a population of solutions and can process a number of solutions in parallel, so it is particularly suited for multi-objective problems. Recently, some competent genetic algorithms [*Goldberg*, 2002], far superior to the conventional genetic algorithm, have been proposed and can solve hard problems quickly, reliably and accurately. *Du et al.* [2002] used GA inversion of SWD to obtain a smooth reference model which was later used as constraint in the linearized inversion of RFs. Here we invert both RFs and SWD simultaneously using one of the competent genetic algorithms, Bayesian optimization algorithm (BOA) [*Pelikan*, 1999, 2001], as the main inversion procedure to sample diverse optimal models under acceptable levels. With multi-objective criteria, the chosen models showed the resolution and extent of solutions in objective-space and model-space areas.

2. Methods

[4] Evolution/genetic algorithms work with a number of solutions or individuals collectively known as a population. The probability distribution of the promising models in a population tells the algorithm where to look for future better solutions. A traditional GA [*Goldberg*, 1989] evolves a population of solutions by repeatedly applying the operators of selection, mutation, and crossover. These solution (and problem) independent operators often break good partial solutions and result in an inferior performance or convergence to a local minimum even in simple problems [*Pelikan et al.*, 1999] because the algorithm does not know the positions of the good genes. Bayesian optimization algorithm (BOA) [*Pelikan et al.*, 1999, 2001], one of the competent GAs, uses Bayesian networks to encode the dependencies between genes of promising solutions and subsequently guide the exploration of search space. The actual difference between BOA and a simple GA is that a Bayesian network is first constructed as a probability model of promising solutions instead of processing selected parent models using crossover and mutation. Then, new candidate solutions are generated using the constructed Bayesian network. More detail about BOA is available elsewhere [*Pelikan et al.*, 1999, 2001].

[5] We added a local trial-and-error jumping iteration [*An and Assumpção*, 2001] to hybridize BOA. In each generation the good models, with misfit less than the average misfit of the last generation, are perturbed by changing their parameter vector in a random direction. If this initial perturbation makes the misfit worse, the perturbation is changed to the opposite direction. Then the perturbation amplitude increases exponentially until the model stops

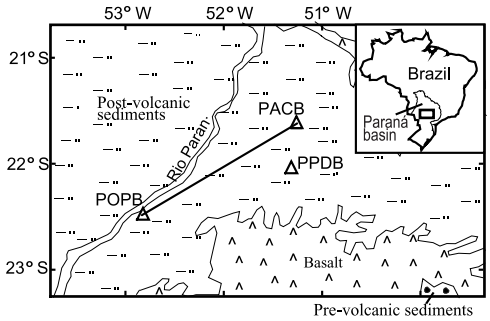

Figure 1. The geological map [*Schobbenhaus and Bellizzia*, 2001] and stations (triangles) in this study.

improving. This local iteration can improve GA's efficiency and model diversity [*An and Assumpção*, 2001].

[6] In the joint optimization, we used two L2-norm objectives: to minimize the misfit of surface wave dispersion (Obj_dispersion) and the amplitude misfit of receiver function (Obj_receiver). The forward procedures of RF and SWD are from Robert B. Herrmann [2003] (www.eas.slu.edu/People/RBHerrmann/index.html). We used the sum of weighted objective functions as the single-objective optimization criterion, and several weights were used to extend the optimal front in the objective-space. This treatment is also effective for conflicting objectives, e.g., observations with strong noise and uncertainties. Using synthetic tests, we found that BOA can get more evenly-distributed models near the optimal solution than traditional GA. The local trial-and-error jumping iteration can help BOA reach the synthetic solution quickly, and still prevent premature convergence to a local solution.

3. Observation, Inversion and Results: Paraná Basin, Brazil

[7] The intracratonic Paraná basin started subsidence in the Early Paleozoic and had several depositional sequences before Cretaceous. The mechanism that caused the initial Paleozoic subsidence is still unclear and different processes have been proposed [e.g., *Pysklywec and Quintas*, 2000]. In Early Cretaceous (~137–130 Ma), just prior to the South Atlantic opening, a large volume of basalt flow covered the entire basin reaching thicknesses up to 1.5 km near the path POPB-PACB (Figure 1). Hence complex basaltic underplating/intrusion and metamorphism in the lower crust could be expected. The center of the Paraná basin has a thicker crust, despite its low altitude, compared to the neighboring foldbelt and craton [*Assumpção et al.*, 2002]. A higher density lower crust (underplated?) would be able to explain such difference. For these reasons, studies of crustal structure in the basin may help to understand more about these questions.

[8] In this study, we used the inter-station Love and Rayleigh phase velocities from *An and Assumpção* [2004] as the surface wave observation. To avoid the influence of lateral heterogeneity, we only selected the path POPB-PACB which did not show obvious lateral heterogeneity in the analysis of SWD [*An and Assumpção*, 2004] and RFs. Using good quality seismograms, the radial (unnormalized) RFs of POPB, PACB and PPDB stations were calculated by the iterative time-domain deconvolution procedure [*Ligorría and Ammon*, 1999]. We used about six events for each station in narrow distance ranges (49°–62° for PPDB, 30°–40° for POPB and 38°–43° for PACB), and m_b magnitude larger than 5.5. The small number of events for each station does not allow to improve signal-to-noise ratio by averaging receiver functions in a limited range of back-azimuths. For each station, the average of all RFs was taken as the observation (Figure 2). According to the observation errors, we determined the acceptable levels for Obj_dispersion as 0.035 km/s, and Obj_receiver as 0.06 s^{-1}. Hence, all sampled models with Obj_dispersion $\leq$ 0.035 km/s or Obj_receiver $\leq$ 0.06 s^{-1} were saved.

[9] The model consisted of six main-layers (at least three in the crust). Each main-layer was parameterized into S-velocities at the layer top and bottom boundaries, thickness and Vp/Vs. Each main-layer was divided into nine homogeneous sub-layers with Vs varying linearly from top to bottom. P-velocity (Vp = Vs × Vp/Vs) and density (calculated from Vp) were varied linearly too. All parameters are listed in Table 1. The population size of BOA is 100 (50% is kept in next generation), and the local trial-and-error iteration will evaluate about 150 more models in each generation. Five objective weight ratios of RF to SWD from 0.6:1 to 100:1 were used. For each ratio, the maximum number of generations is 100.

[10] The inverted results of station PPDB are shown in Figure 3. Figure 3b shows that the inverted models only constrained by RF have a sharp discontinuity in the crustal base, caused by the strong Ps phase in RF observation. The models only constrained by SWD (Figure 3d) show the general S-velocity trend with depth. Figure 3e shows all (>100,000) models in the objective-space. The models with Obj_dispersion >0.035 km/s and Obj_receiver >0.06 s^{-1} are outside the acceptable levels of both RF and SWD, and are not shown. The irregular optimal front in Figure 3e does not imply front complexity but model-sampling insufficiency. This figure shows that a model fitting well one objective can fit the other objective badly, so a multi-objective criterion of RF and SWD is necessary to select the acceptable models. We chose a criterion MultiObj = 4 × Obj_

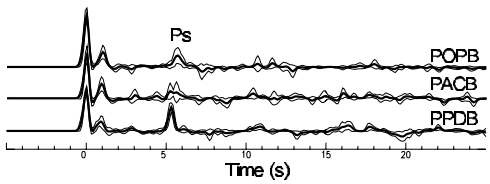

Figure 2. The average (thick lines) and standard deviations (thin lines) of RFs for each station. Ps phase is the P-to-S conversion at the Moho.

Table 1. Search Range [Minimum-Maximum] and String Length of the Model Parameters

Layer	Thickness	Vs (top)	Vs (bottom)	Vp/Vs
1	1–6 km; 8	2.4–3.8 km/s; 8	–	1.8
2	5–30 km; 10	2.6–3.4 km/s; 10	3.0–4.0 km/s; 10	1.6–1.9; 5
3	5–30 km; 10	3.2–4.2 km/s; 10	3.2–4.2 km/s; 10	1.6–1.9; 5
4	5–100 km; 10	3.2–4.2 km/s; 10	3.5–5.0 km/s; 10	1.6–1.9; 5
5	5–80 km; 10	3.5–5.0 km/s; 10	3.5–5.5 km/s; 10	1.78
6	half space	3.5–5.5 km/s; 10	–	1.8

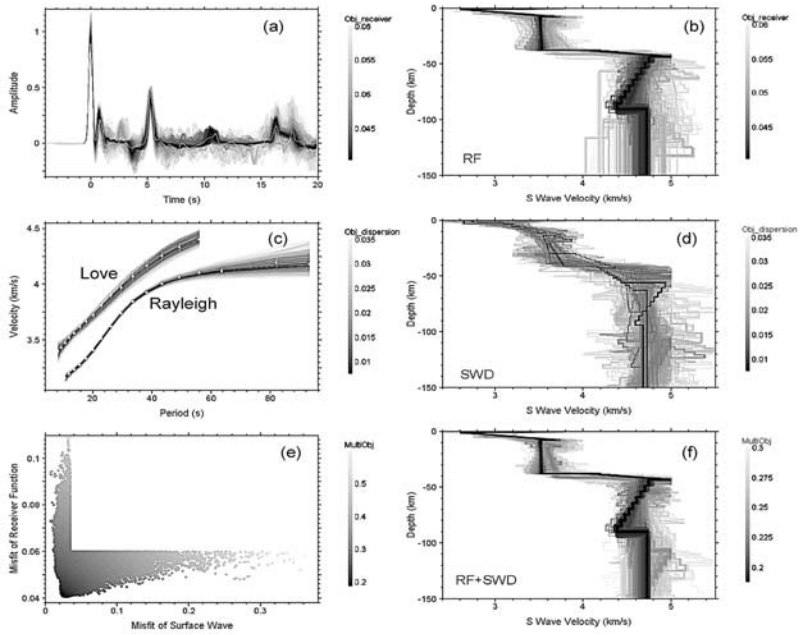

Figure 3. The PPDB inverted models (b, d, f), fitness (a, c) and the objective-space (e). The gray scale (color) beside each diagram is the model misfit. Obj_receiver is the objective function (misfit) of receiver function, Obj_dispersion is of surface wave dispersion. The observation of RF is the white line (black) in (a), and of SWD is the white points (black) with error bars in (c). See color version of this figure in the HTML.

receiver + Obj_dispersion, with the relative weight (4:1) giving slightly more importance in fitting the receiver function which is related to the structure directly beneath the station compared to inter-station SWD. Figure 3f shows the models constrained by MultiObj <0.3. The combination of the relative weight (4:1) with the limiting value MultiObj = 0.3 allows the selection of models with one objective slightly above its acceptable limit (e.g., Obj_dispersion >0.035 km/s) but close to the minimum of the other objective in Figure 3e. These models have good resolution down to about 150km and show the common features of the good models in Figures 3b and 3d. Without much more sampling computation, the multi-objective criterion of RF and SWD eliminated the unacceptable models in Figures 3b and 3d.

[11] Figure 4 shows the profiles of the fitness (MultiObj^{-1})-weighted average S-velocities of the accepted models. In Figure 4, the topmost, thin ($\sim$1.8 km) high-velocity layer corresponds to the basalt flood cover plus the thin ($<\sim$500 m) post-volcanic sediments in the Paraná basin. Just under this layer, the lowest velocity should correspond to the pre-volcanic sediments. The large peak at $\sim$1 s in the RFs (Figure 2) is the P-to-S conversion at the sediment/basement interface, which was modeled as a steep gradient in our inversion (Figure 3f). Below the depth of 40 km, Vs changes from the lower crust smoothly to the upper mantle, especially for POPB and PACB (Figure 4). For stations POPB and PACB, the amplitudes of Ps phases at $\sim$5.5 s (Figure 2) do not require a sharp Moho.

4. Discussion

[12] Because we inverted the average of RFs from all back-azimuth, the results show the general trend of the average profile beneath each station. Velocities less than 3.8 km/s in Figure 4 in the lower crust seem to be characteristic of the Paraná basin. Other studies have indicated similar results. Surface wave dispersion for other inter-station pairs covering other parts of the Paraná basin [*Assumpção et al.*, 2002; *An and Assumpção*, 2004] showed average S-velocity less than 3.8 km/s between 20 and 40 km depth. Surface-wave tomography of the South American continent [*Feng et al.*, 2003] also indicated lower average S-wave velocities at 30 km depth beneath the Paraná basin relative to high velocities in the surrounding fold belts. These results may indicate that the lower crust beneath the Paraná basin has a more felsic composition compared to the foldbelts around it.

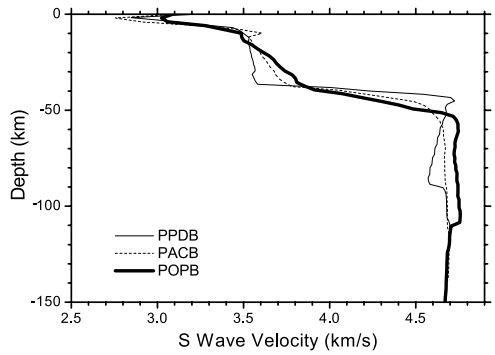

Figure 4. The fitness-weighted average of S-velocities in each depth from all acceptable models. The PPDB profile is the fitness-weighted average from all models in Figure 3f. The other two profiles were obtained in the same way from the acceptable models with the same MultiObj criterion by fitting the surface wave dispersion and the respective receiver function in Figure 2.

[13] A high velocity layer in the lowermost crust (Vp > 7.0 km/s, Vs > 4.0 km/s), up to 10 km thick, is often observed in large sedimentary basins and areas of continental rift, and is often attributed to underplating [e.g., *Mooney et al.*, 1983; *Durrheim and Mooney*, 1994]. *Molina et al.* [1988] modeled a 25–30 mGal gravity high along the axis of the northern Paraná basin as due to a high-density 12 km thick layer in the lowermost crust, interpreted as evidence for underplating. Our profiles in Figure 4, however, only show a gradual Moho which could be interpreted as thin high-velocity layer in the lowermost crust. The profile of PPDB shows a sharp transition from lower crust (S-velocity <4.0 km/s) to upper mantle (>4.4 km/s). Station POPB shows a more gradual transition with high velocities (4.0 to 4.4 km/s) from 40 to 47 km depth. PACB shows the mean properties of POPB and PPDB below the depth of 20 km. POPB-PACB is near the center of the Paraná basin where the basalt flow is thickest. However, averaging RFs from different back-azimuth could cause some smoothing due to possible lateral variation. For this reason, the ''thicknesses'' of the Moho transitions in Figure 4 are upper bounds. So, our results indicate that possible underplating processes accompanying the basalt extrusion during the South Atlantic rifting was not widespread in the Paraná basin but limited and localized in some areas.

[14] **Acknowledgments.** Work financed by grants 01/06066-6 and 00/07134-2 (FAPESP-Brazil). We thank Robert B. Herrmann for discussions on seismic data analyses and sharing his seismological programs. We also thank Martin Pelikan and David E. Goldberg for suggestions on the genetic algorithms and sharing their BOA codes. Two anonymous reviewers are thanked for their insightful comments and suggestions.

References

An, M., and M. Assumpção (2001), Surface wave dispersion inversion using improved genetic algorithm, paper presented at 7th International Congress of the Brazilian Geophysical Society. SBGf, Salvador, Brazil, Oct. 2001.

An, M., and M. Assumpção (2004), Crust and upper mantle structure in intracratonic Paraná basin from surface wave dispersion using genetic algorithm, submitted to *J. South Am. Earth Sci.*

Assumpção, M., D. E. James, and J. A. Snoke (2002), Crustal thicknesses in SE Brazilian shield by receiver function analysis: Implications for isostatic compensation, *J. Geophys. Res.*, *107*(B1), 2006, doi:10.1029/2001JB000422.

Du, Z. J., and G. R. Foulger et al. (2002), Crustal structure beneath western and eastern Iceland from surface waves and receiver functions, *Geophys. J. Int.*, *149*, 349–363.

Durrheim, R. J., and W. D. Mooney (1994), Evolution of the Precambrian lithosphere: Seismological and geochemical constraints, *J. Geophys. Res.*, *99*(B8), 15,359–15,374.

Feng, M., M. Assumpção, and S. Van Der Lee (2003), Surface wave group velocity tomography and lithospheric S-velocity structure of South American continent, *Eos Trans. AGU*, *84*(46), Fall Meet. Suppl., Abstract S41D-0109.

Goldberg, D. E. (1989), *Genetic Algorithms in Search, Optimization, and Machine Learning*, Addison-Wesley, Reading, MA.

Goldberg, D. E. (2002), *The Design of Innovation: Lessons from and for Competent Genetic Algorithms*, Genetic Algorithms and Evolutionary Computation (7), Kluwer Academic Pub., Boston.

Julià, J., C. J. Ammon, R. B. Herrmann, and A. M. Correig (2000), Joint inversion of receiver function and surface wave dispersion observations, *Geophys. J. Int.*, *143*, 99–112.

Ligorría, J. P., and C. J. Ammon (1999), Iterative deconvolution and receiver function estimation, *Bull. Seism. Soc. Am.*, *89*, 1395–1400.

Molina, E. C., N. Ussami, N. C. de Sá, D. Blitzkow, and O. F. Miranda Filho (1988), Deep crustal structure under the Paraná Basin (Brazil) from gravity study, In *The Mesozoic Flood Volcanism of the Paraná Basin: petrogenetic and geophysical aspects*, edited by E. M. Piccirillo and A. J. Melfi, 271–283, Universidade de São Paulo, São Paulo.

Mooney, W. D., M. C. Andrews, A. Ginzburg, D. A. Peters, and R. M. Hamilton (1983), Crustal structure of the Mississippi embayment and a comparison with other continental rift zones, *Tectonophysics*, *94*, 327–348.

Özalaybey, S., M. K. Savage, A. F. Sheehan, J. N. Louie, and J. N. Brune (1997), Shear-wave velocity structure in the northern Basin and Range province from the combined analysis of receiver functions and surface waves, *Bull. Seism. Soc. Am.*, *87*, 183–199.

Pelikan, M., D. E. Goldberg, and E. Cantú-Paz (1999), BOA: the Bayesian optimization algorithm, in *GECCO '99: Proceedings of the Genetic and Evolutionary Computation Conference*, edited by W. Banzhaf, J. Daida, A. E. Eiben, M. H. Garzon, V. Honavar, M. Jakiela, and R. E. Smith, 525–532, Morgan Kaufmann, San Francisco, CA.

Pelikan, M., D. E. Goldberg, and K. Sastry (2001), Bayesian optimization algorithm, decision graphs, and Occam's razor, in *GECCO 2001: Proceedings of the Genetic and Evolutionary Computation Conference*, edited by L. Spector and E. D. Goodman, 519–526, Morgan Kaufmann, San Francisco, CA.

Pysklywec, R. N., and M. C. L. Quintas (2000), A mantle flow mechanism for the late Paleozoic subsidence of the Paraná Basin, *J. Geophys. Res.*, *105*(B7), 16,359–16,370.

Schobbenhaus, C., and A. Bellizzia (2001), Geological Map of South America, 1:500,000, CGMW-CPRM-DNPM-UNESCO, Brasilia.

M. An and M. S. Assumpção, Department of Geophysics, IAG, University of São Paulo, Rua do Matão 1226, São Paulo, SP, 05508-090, Brazil. (meijian@iag.usp.br; marcelo@iag.usp.br)